

Improving ecological inference and uncertainty quantification from camera trap data through the fusion of AI confidences and manual annotations

Adira Cohen¹, Erin M. Schliep¹, Roland Kays^{2,3},
Mohammad Alyetama^{2,4}, and Matthew Snider²

¹North Carolina State University, Raleigh, NC, USA

²Department of Forestry and Environmental Resources, North Carolina State University, Raleigh, NC, USA

³North Carolina Museum of Natural Sciences, Raleigh, NC, USA

⁴Department of Psychology, Neuroscience and Behavior, University of Nebraska Omaha, Omaha, NB, USA

May 14, 2026

Abstract

Camera traps have become a core tool in ecological research, enabling large-scale, noninvasive monitoring of wildlife populations and behavior. By automatically recording animals as they pass within view, these devices generate massive image datasets with minimal field effort. Yet this data richness introduces a new bottleneck when translating the images into usable information due to time and

effort required for human annotation. Recently, artificial intelligence (AI) has been integrated into the workflow to improve efficiency. However, the data procured from AI approaches are of a different nature, necessitating new statistical methods to obtain inference, make predictions, and quantify uncertainty. We propose a new Bayesian hierarchical data-fusion model that combines the strengths of human annotations and AI predictions. The benefits of our approach are an ability to provide uncertainty quantification as well as improved inference and prediction power, which we demonstrate using a simulation study. We apply our model to an AI analysis of the body condition of white-tailed deer (*Odocoileus virginianus*) from camera trap images from North Carolina to study the relationship between health and their environment. We find that bucks in rut have higher body condition than other deer and that green, open habitats are correlated with high body condition. Our new model derived novel ecological inference compared to a traditional approach using the same data.

1 Introduction

Camera traps and automated sound recording units have revolutionized the sampling of wildlife populations due to their low cost and noninvasive nature. The recordings of species presence can be used for distribution studies and population monitoring via occupancy and abundance modeling [e.g., Goldstein et al., 2024, Schliep et al., 2024]. Photo captures can also be used to study animal body condition and diseases [e.g., Muneza et al., 2019, Ringwaldt et al., 2025]. Improved statistical approaches enable the use of these devices at a larger scale. The increased scale is beneficial for ecology and conservation efforts but has led to challenges in processing the larger volumes of data [Leorna and Brinkman, 2022, Delisle et al., 2021, Terry et al., 2020]. Specifically, identifying the species — or otherwise characterizing the data from the image or sound — requires extensive manual work.

Artificial intelligence (AI) is useful for quickly processing the large datasets, enabling the continued increase of the scale of surveys. The use of convolutional neural networks, a popular type of AI model, for image classification have grown rapidly over the past decade [Oliveira et al., 2025]. AI models using camera trap data have been shown to be effective for filtering blanks [e.g., Mulero-Pázmány et al., 2025, Henrich et al., 2024] and species identification [e.g., Lonsinger et al., 2024, Mulero-Pázmány et al., 2025], as well as disease detection [e.g., Ringwaldt et al., 2025] and distance estimation [e.g., Henrich et al., 2024].

While AI predictions provide a solution to the annotation bottleneck, statistical methods using AI-integrated camera trap datasets have not kept pace. This is in part due to a lack of standardization in the output from AI models, including how AI confidences are used and interpreted [Cowans et al., 2024]. Statistical models that do exist [e.g., Rhinehart et al., 2022, Cole et al., 2022] tend to only be applicable to unrealistically simplified study scenarios.

Properly integrating AI predictions into statistical models is a challenging task. To this end, a variety of approaches have been proposed with differing advantages and disadvantages. First, the typical approach is to consider only the most confident AI predictions and discard low confidence results and manual annotations [e.g., Lin et al., 2021, Schwob et al., 2025], mirroring models for compositional data [e.g., Feng et al., 2017]. The disadvantage of this approach is that some data are discarded, and that AI accuracy tends to be lower than human accuracy for all but simple tasks [Kitzes et al., 2025]. Moreover, unlike statistical models, AI confidences are not generally *calibrated* (i.e., converted to probabilities). Building probabilistic models that properly quantify uncertainty using AI confidences necessitates the use of additional data, such as manual annotations [Dussert et al., 2025, Kitzes et al., 2025].

Other analyses fit models separately to AI predictions and manual annotations [e.g., Cole et al., 2022, Lonsinger et al., 2024, Ringwaldt et al., 2025, Henrich et al., 2024], which

allows for some uncertainty quantification through model comparison. These studies show that although AI predictions have more noise than manual annotations, they can produce comparable results given enough data. While an improvement, this approach is not ideal because it does not collectively leverage the unique strengths of each dataset. There is no direct sharing of information between models, so that the models fit on the AI predictions lack uncertainty quantification and the models fit on the manual annotations are limited by study scale.

A third approach uses manual annotations to calibrate the AI confidences, which converts the AI confidences into probabilities [e.g., Ware et al., 2023, Wood et al., 2024]. This provides a valuable improvement by using the strengths of each data type to quantify uncertainty in the model. However, proper uncertainty propagation is challenging in this two-stage procedure.

Lastly, models that jointly use both AI predictions and manual annotations, often referred to as data fusion models, have recently been developed [e.g., Rhinehart et al., 2022, Doser et al., 2021]. This approach is common in other applications when there is one abundant but poor-quality data source and a second source that is scarce but of high quality [e.g., Zaiats et al., 2024]. In this case the data sources are also different in nature, as manual annotations are ordinal (integers) while the AI outputs a compositional vector conveying its confidence of each possible ordinal score. Joint modeling allows the strengths and weaknesses of each data source to complement each other, where the manual annotations provide calibration and uncertainty quantification, and the AI confidences provide massive amounts of inexpensive data. However, the disparate data types necessitate new statistical methods to obtain inference, make predictions, and quantify uncertainty.

The current approaches are limited in that they either discard valuable sources of uncertainty — such as manual annotations, the distribution of AI confidences, or via thresholding — or do not fully leverage the available data to improve inference and

prediction. To address these concerns, we propose a Bayesian hierarchical data-fusion model which combines the strengths of human annotations and AI predictions. The benefits of our approach are an ability to provide uncertainty quantification and improved inference and prediction power. We incorporate the nature of the data, in particular modeling the AI outputs as confidences rather than probabilities. Our analysis uses camera trap data from the Candid Critters project [Lasky et al., 2021], which encompasses all of North Carolina. We are interested in using the images from this study to understand the relationship between the body condition of white-tailed deer and their environment.

In Section 2 we describe the Candid Critters dataset and the two sources of data – human annotations and AI confidences. We present our proposed data fusion model in Section 3, and include details on model fitting and inference. In Section 4 we include a simulation study to demonstrate the strength of our approach. In Section 5, we present the results from fitting our model to the Candid Critters dataset. We conclude with a discussion of our model and results in Section 6.

2 Description of the data

2.1 Camera traps and Candid Critters

Candid Critters was an organized citizen science camera trapping project across North Carolina with participants from all 100 counties [Lasky et al., 2021]. There are 4295 deployments (camera placements) from 2016 to 2019, the locations of which are shown in Figure 1. The cameras were placed on both private and public land with retrievals collected from all seasons. The cameras were set at least 200m apart without bait, and were pointed away from high-traffic regions such as a bird-feeders, game-trails, or roads. The cameras used were motion-sensitive infrared flash trail cameras, meaning that they are triggered by movement of heat (such as a mammal walking in front of the camera) and are able to take images during the day or night. When triggered, the cameras

take 5 photographs at approximately 1 second intervals for each trigger, and retrigger immediately if the animal is still present, resulting in a *sequence*. Over the span of the Candid Critters project, 2.2 million images of wildlife were collected, 56% of which were white-tailed deer (*Odocoileus virginianus*, hereafter “deer”), our species of interest. The large number of images of deer creates problems of human effort when annotating images, which motivates our analysis.

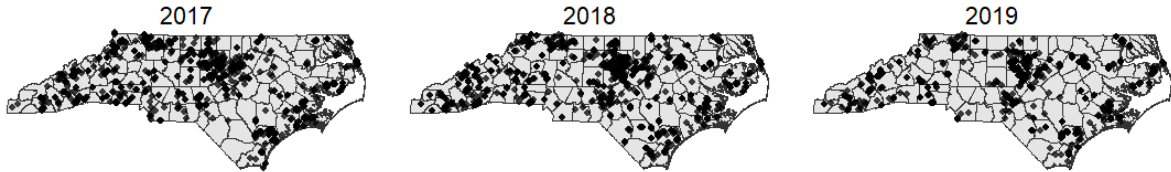


Figure 1: Deployment locations for Candid Critters dataset, which spans North Carolina, after data cleaning separated by year. There are at total of 104464 images representing 17471 sequences at 2766 deployments.

Within each sequence there are multiple images, each of which may either be blank or contain one or more individuals. Each individual animal is given a bounding box to identify its location in the image. For our analysis, species and group size were already manually annotated for each sequence. With group sizes of 1, the sequence is a repeated survey of a single individual. For larger groups, it is impossible to accurately track individuals across frames, so we do not include these in our analysis.

2.2 Deer body condition score and manual annotations

Body Condition Score (BCS) is a measure designed to assess certain health indicators of white-tailed deer, such as the appearance of the ribs, spine, and belly [Smiley, 2017, McGraw et al., 2022]. The BCS takes on ordinal integer values of 1, 2, 3, 4, or 5, where 1 is the least healthy and 5 is the most healthy. A deer with a BCS of 1 appears extremely thin and bony whereas a deer with a BCS of 5 appears plump. See Figure 2 for an

example of each ordinal category.



Figure 2: Images of white-tailed deer taken by camera traps labeled with their body condition score.

The human annotated data used in our analysis were obtained from a team of researchers who were trained in scoring body condition. The annotators scored unique partitions of images (i.e., each image was scored by at most one annotator), and each image was viewed independently without considering other images in the sequence. This is the slowest yet most reliable method, although the annotators are fallible and may have some individual classification bias.

2.3 AI model

An image can be assigned a set of confidences by an artificial intelligence (AI) model. This method is much faster than manual annotations but less reliable. In addition to inherent classification error through AI, the precision of the AI confidences may vary depending on factors such as light exposure. The data used in our analysis came from applying an AI model trained to score the body condition of deer [Alyetama and Snider, 2024] to images of deer from the Candid Critters dataset. The first AI sub-model accepts individual images of deer as input and filters them using a convolutional neural network to predict image quality. High-quality images are passed to another AI sub-model which classifies the BCS of each deer. For each image the AI model provides compositional data consisting of a vector of confidences of the BCS being in each ordinal category. The confidences must sum to 1 and higher values denote higher confidence. For example, an

AI confidence of $[0, 0.1, 0.7, 0.2, 0]$ implies that the model is most confident that the deer has BCS 3, with lower confidence for scores of 2 and 4.

The AI model significantly increases the amount of data while decreasing the time frame of the project with respect to both human effort and amount of time until the data are available. The AI model scored all 104464 images of solitary deer in the Candid Critters dataset in approximately 40 minutes with almost no human effort, whereas it would have taken over 5 months of dedicated human effort to score these images by hand. These images represent 17471 sequences at 2766 deployments, which contain 92 manual annotations and 104464 AI confidences. Importantly, we do not use any images in our analysis that were used to train the AI model.

2.4 Ecology model

We are interested in understanding how the body condition of deer is related to certain individual and environmental drivers. Life stages of deer are known to be important drivers of variation in body structure. We classify deer as being a buck during rut if they are a male deer captured in October to December. If the deer is captured during this time period then the deer is sexed using an AI model [Alyetama and Snider, 2024], and being a buck during rut or not is equivalent to being male versus female. Otherwise, all deer are classified as not being a buck during rut, since deer without antlers are difficult to sex. Bucks during rut are expected to have the highest body condition because they spend the previous months gaining weight to compete for does. We also consider other landscape variables such as deer relative abundance (at 10 km resolution) [from Kays et al., 2024], county-level human population density [from U.S. Census Bureau], landscape diversity (at 1km resolution) [from Jung et al., 2020], normalized difference vegetation index (NDVI) (at 1km resolution) [from Dodge et al., 2013], and percent of tree canopy cover (at 30m resolution) [from Sexton et al., 2013]. All environmental covariates are constant in time except NDVI, which is sampled in monthly intervals. To

differentiate between high NDVI caused by forest (which may not be accessible by deer) from short vegetation, NDVI and tree canopy are combined using principal component analysis (PCA). The first component measures how green (high NDVI) and open (low tree canopy value) the habitat is and the second component measures how green and forested (high tree canopy value) the habitat is. We expect that deer will have higher body condition in areas with green and open habitat because higher values indicate larger amounts of accessible vegetation. The spatial distributions of the environmental drivers across North Carolina are given in Figure 3. The environmental drivers are centered and scaled before fitting the model.

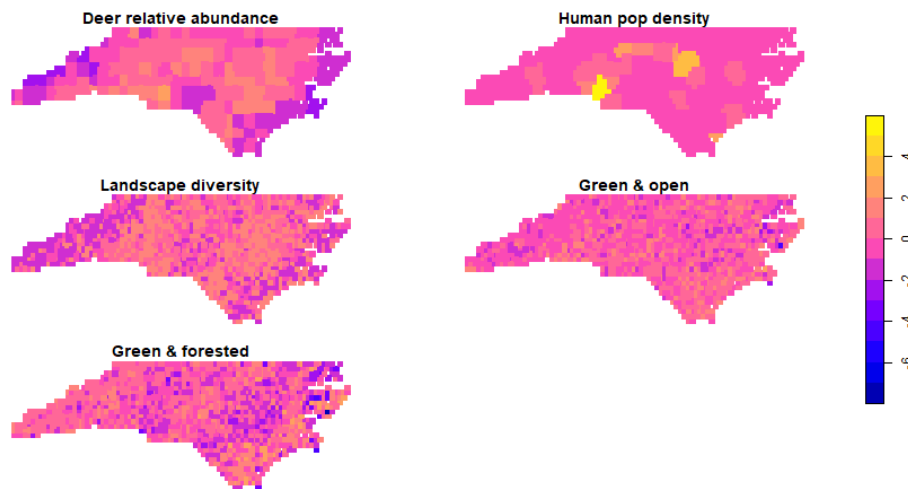


Figure 3: Maps of environmental covariates after centering and scaling, where the NDVI values used to calculate “green & open” and “green & forested” are sampled from November 2018 as an example.

3 Fusion model specification and inference

3.1 Model framework

In this section we describe the general modeling framework given the two sources of data. We develop a hierarchical model that links the true, unobserved BCS for each individual to two imperfect observation sources — manual ordinal annotations and AI-derived

compositional confidences — while simultaneously relating the latent score to ecological covariates. The framework accounts for annotation error, annotator heterogeneity, AI uncertainty, and the ordinal structure of the biological process. A basic layout of the framework is given in Figure 4. Refer to Table 5 in Section S.1 for a description of all data and parameters.

Let N be the number of sequences, where each sequence contains one individual. We assume that each individual has a true latent ordinal BCS which represents the health of the individual. Let $r_i > 0$ denote the number of images for sequence $i = 1, \dots, N$. Therefore the total number of images is $R = r_1 + \dots + r_N$. Define Λ_i^Z and Λ_i^C as the set of indices within sequence i that are manually annotated or scored by AI, respectively. Note that the length of the union of these two sets is equal to r_i , either could be empty, and their intersection need not be empty. This implies that all images produce at least one form of observation and some images can have both annotated and AI observations.

Let L denote the number of ordered categories of BCS, where $L \geq 2$. For manual annotations, define $Z_{i,k} \in \{1, \dots, L\}$ for image $k \in \Lambda_i^Z$ of sequence i . Let $\mathbf{C}_{i,k}$ be the L -length compositional AI confidence for image $k \in \Lambda_i^C$ of sequence i . We say that an L -length vector is compositional if it belongs to the $(L - 1)$ -dimensional simplex (i.e., all elements are nonnegative and sum to 1).

The observed manual annotations and AI confidences are modeled as function of the true BCS. Let $Y_i \in \{1, \dots, L\}$ for $i = 1, \dots, N$ denote the true latent BCS for individual i . For the ordinal manual annotations, we assume a probit link function and model $Z_{i,k}$

$$\begin{aligned} f_Z(z|Y_i, \boldsymbol{\nu}, \boldsymbol{\phi}) &= \mathbb{P}(Z_{i,k} = z|Y_i, \boldsymbol{\nu}, \boldsymbol{\phi}) \\ &= \int_{\phi_{Y_i, z-1}}^{\phi_{Y_i, z}} \frac{1}{\sqrt{2\pi}} \exp \left[-\frac{1}{2} \left(t - \nu_{Y_i}^{(a_{i,k})} \right)^2 \right] dt \\ &= \Phi \left(\phi_{Y_i, z} - \nu_{Y_i}^{(a_{i,k})} \right) - \Phi \left(\phi_{Y_i, z-1} - \nu_{Y_i}^{(a_{i,k})} \right) \end{aligned} \quad (1)$$

where Φ is the cumulative distribution function for a standard normal random variable.

Here, $a_{i,k}$ indexes the annotator for image k of sequence i . The annotation probabilities are controlled by annotator- and BCS-specific means $\nu_{Y_i}^{(a_{i,k})}$ and cutoffs $-\infty = \phi_{y,0} < \phi_{y,1} < \dots < \phi_{y,L-1} < \phi_{y,L} = \infty$ for $y = 1, \dots, L$. Annotator-specific parameters allow for variation in accuracy across annotators assumed to be present in the data. We assume independence across scores within annotators, although this assumption could be relaxed to incorporate dependence as desired.

The AI derived compositional data, $\mathbf{C}_{i,k} = (c_{i,k,1}, \dots, c_{i,k,L})$, are modeled using independent Dirichlet distributions with mean $\boldsymbol{\alpha}_y$ and precision $\exp[\omega_0 + \mathbf{U}_{i,k}^\top \boldsymbol{\omega}]$, where $\mathbf{U}_{i,k}$ are possible image-quality covariates for image k of sequence i and $\omega_0, \boldsymbol{\omega}$ are coefficients. Therefore the probability distribution function for the compositional AI responses for image $k \in \boldsymbol{\Lambda}_i^C$ of sequence i is

$$f_C(\mathbf{c}|Y_i, \boldsymbol{\alpha}, \boldsymbol{\omega}) = \left(\frac{\Gamma(\exp[\omega_0 + \mathbf{U}_{i,k}^\top \boldsymbol{\omega}])}{\prod_{\ell=1}^L \Gamma(\exp[\omega_0 + \mathbf{U}_{i,k}^\top \boldsymbol{\omega}] \boldsymbol{\alpha}_{Y_i, \ell})} \right) \prod_{\ell=1}^L c_\ell^{\exp[\omega_0 + \mathbf{U}_{i,k}^\top \boldsymbol{\omega}] \boldsymbol{\alpha}_{Y_i, \ell} - 1}. \quad (2)$$

We restrict $\boldsymbol{\alpha}_\ell$ to the $(L-1)$ -dimensional simplex so that it is a valid mean for $\mathbf{C}_{i,k}$. The precision controls how tightly the values cluster around the mean, where higher precisions correspond to more consistent AI confidences within the sequence.

Finally, we turn to modeling the latent process, Y_i , which captures the relationship between true BCS and possible individual level and environmental covariates. Using a probit regression model [Albert and Chib, 1993], we define

$$\begin{aligned} f_Y(y|\beta_0, \boldsymbol{\beta}, \boldsymbol{\theta}) &= \mathbb{P}(Y_i = y|\beta_0, \boldsymbol{\beta}, \boldsymbol{\theta}) \\ &= \int_{\theta_{y-1}}^{\theta_y} \frac{1}{\sqrt{2\pi}} \exp\left[-\frac{1}{2} (t - \beta_0 - \mathbf{X}_i^\top \boldsymbol{\beta})^2\right] dt \\ &= \Phi(\theta_y - \beta_0 - \mathbf{X}_i^\top \boldsymbol{\beta}) - \Phi(\theta_{y-1} - \beta_0 - \mathbf{X}_i^\top \boldsymbol{\beta}) \end{aligned} \quad (3)$$

where \mathbf{X}_i^\top is a length p vector of covariates for sequence i , β_0 and $\boldsymbol{\beta}$ are the set of regression coefficients, and $-\infty = \theta_0 < 0 = \theta_1 < \dots < \theta_{L-1} < \theta_L = \infty$ are the cutoffs

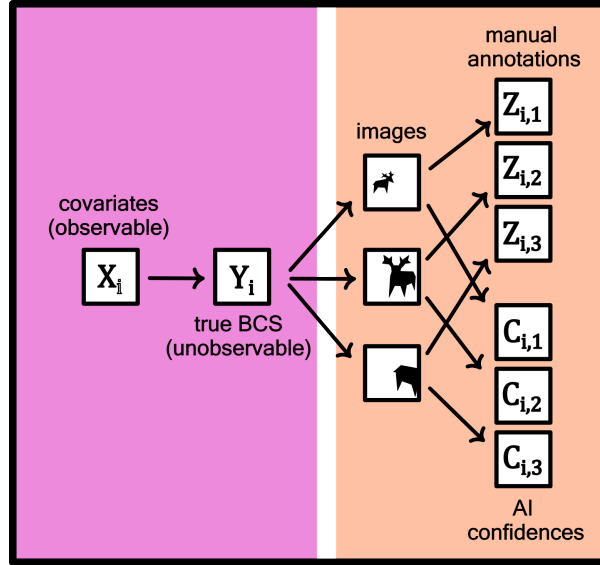


Figure 4: Hierarchical model framework for an arbitrary sequence i .

between the latent ordinal variables.

3.2 Model inference

We specify our model hierarchically and obtain inference through a Bayesian framework. Prior distributions are assigned to all model parameters. We assign independent normal prior distributions with mean zero and variance 1 to each coefficient parameter, β_1, \dots, β_p . Normal priors with mean 0 and variance 10 are assigned to β_0, ω_0 , and $\omega_1, \dots, \omega_q$. For parameter identifiability, we fix $\theta_1 = \phi_{1,1} = \dots = \phi_{L,1} = 0$ without loss of generality. For computational efficiency, θ and ϕ are both reparameterized to alleviate the restricted distributions such that $\theta_y = \theta_{y-1} + e^{\tilde{\theta}_y}$ for $y = 2, \dots, L - 1$ and $\phi_{y,z} = \phi_{y,z-1} + e^{\tilde{\phi}_{y,z}}$ for $y = 1, \dots, L$ and $z = 2, \dots, L - 1$. The priors for these cutoff parameters are Log-Normally distributed with variance 10. The means for θ are equally spaced and chosen such that the *a priori* probability that Y_i is in any given category is at most 0.5. The means for ϕ are spaced such that annotators are assumed to be 95% accurate, with equal probability given to all other categories. Because we assume the annotators are relatively consistent, we let the mean $\nu_y^{(a)}$ for each category y and annotator a be

normally distributed centered around some latent $\tilde{\nu}_y$ with small variance 0.2. We let $\tilde{\nu}_y$ be uniformly distributed within its appropriate cutoffs $[\phi_{y,y-1}, \phi_{y,y}]$. Each α_y is a L -length vector where the y th element is 0.4 and all other elements are given equal weight for $y \in \{1, \dots, L\}$. For example, if $L = 5$ then $\alpha_1 \sim \text{Dir}([0.4, 0.15, 0.15, 0.15, 0.15])$. A higher weight on the correct prediction provides model stability and is justified by validation of the AI model, which shows high accuracy. Keeping the precision low and weight evenly spread across scores ensures the prior distribution is relatively uninformative.

Posterior samples are obtained through a customized Markov chain Monte Carlo (MCMC) sampling algorithm. A Gibbs step is used to sample \mathbf{Y} directly, while an adaptive Metropolis-Hastings algorithm is used for the remaining parameters. Details about sampling are given in the appendix. To handle numerical issues with the Dirichlet distribution when an element of $C_{i,k}$ is exactly zero or one, we adjust C by first choosing $\zeta = 1e - 12$ and $\zeta = 1e - 3$ for the simulation study and case study, respectively. Then, for all $\mathbf{C}_{i,k}$ which contain any elements smaller than ζ , ζ is added to each element and divided by the sum of the vector to preserve the unitary sum. This is done for numerical stability of the algorithm and results were found to be robust to this adjustment.

4 Simulation study

The simulation study evaluates how well the full data-fusion model recovers environmental effects and predicts latent BCS relative to simpler modeling shortcuts commonly used in camera-trap AI applications.

4.1 Model settings

The following simulation was conducted to evaluate the proposed modeling approach for the two data sources. To this end, we chose 5 relevant model settings, listed below, for comparison.

Setting 1 (linear) assumes a linear regression model and is one of the simplest approaches one might take to model the data. Under this approach, the ordinal nature of the observed data are ignored and instead, continuous response variables \tilde{Y}_i for $i = 1, \dots, N$ are extracted. If sequence i has annotated images, then all AI confidences are ignored and \tilde{Y}_i is the mean of the annotations. Otherwise, \tilde{Y}_i is the mean of the weighted average of AI confidences for sequence i . All confidences for which the maximum value is less than some prespecified threshold T are discarded prior to computing \tilde{Y}_i to reduce uncertainty following, for example, Cowans et al. [2024] and Ringwaldt et al. [2025]. We model these continuous response variables using a Bayesian linear regression model to enable easy comparison.

Setting 2 (maximum) applies a threshold to the AI confidences to filter out less confident predictions. The manual annotations are ignored. The ordinal value with the maximum confidence is extracted and the median of these values across all images within the sequence is retained as the observed ordinal value for individual i . This is a common interpretation of AI confidences. For simplicity, the model in this setting assumes that Y_i can be observed without error. As with setting 1, AI confidences with maximum value less than T are discarded.

Settings 3-4 use the proposed model from Section 3 but are limited to a single data source. *Setting 3 (ordinal-only)* omits the AI confidences while *setting 4 (compositional-only)* omits the manual annotations. *Setting 5 (full model)* uses all available data under the full proposed model in Section 3. Comparisons between the models under settings 3 and 4 to the full model (setting 5) will highlight the benefits of each data source with regard to model inference and predictions.

4.2 Model comparison

We assess the 5 models based on their ability to address the specific goals of the analysis. First, to assess how well the model estimates the coefficients for the environmental drivers,

the mean squared error (MSE) and empirical coverage for each β are reported under each model setting. Second, to assess the model fit with respect to the true BCS values, Y_1, \dots, Y_N , the ranked probability score (RPS) is calculated with respect to the posterior distribution of \mathbf{Y} given the data. Third, to evaluate the predictive ability of the model, we compute the RPS for each out-of-sample individual at a new location (i.e., using the posterior prediction distribution of \mathbf{Y}_0 given the data, where \mathbf{Y}_0 is the vector of latent true ordinal BCSs for a set of out-of-sample individuals). RPS is a proper scoring rule [Gneiting and Raftery, 2007], meaning it is minimized by the true distribution, that accounts for both accuracy and precision in prediction. The posterior predictive distribution of the ordinal score is compared to the true value of the ordinal data and lower values correspond to better predictions. Details for computing RPS under our model are given in Section S.3. Note that the BCSs for setting 1 are continuous so the RPS analysis is omitted due to lack of comparison.

4.3 Simulation settings

The simulation settings are chosen to mimic realistic ecological data from camera traps. We randomly generate 100 data sets and fit each of the 5 models to each dataset according to the preprocessing outlined in Section 4.1. For each simulation, we assume $N = 500$ training sequences and 1000 testing sequences. For sequence $i \in 1, \dots, N$, the number of images in the sequence, r_i , is randomly assigned a value in the set $\{1, 3, 5, 10\}$ with equal probability. Each image is assumed to have AI confidences whereas a pre-specified proportion of the images are randomly selected to have manual annotations. For settings 3 and 5 we randomly select 10%, 20%, and 50% of the images to manually annotate, and for setting 1 we randomly select 20% of the images to manually annotate. We assume $L = 5$ ordered categories for the latent ordinal process of interest. We set $\beta_0 = 1.38$, $\beta = [0.2, -0.3, 0.0, 0.0, 0.2, -0.3]^\top$, $\omega_0 = 0$, and $\omega = 1$. We fix θ so that the maximum probability of Y_i being in categories 2, 3, and 4 are 0.2, 0.5, and 0.3,

respectively. Similarly, we assume there are 3 annotators and fix $\tilde{\nu}$ and ϕ such that an annotator with $\nu^{(a)} = \tilde{\nu}$ would be 95% accurate, and randomly generate each $\nu^{(a)} \sim \text{MVN}(\tilde{\nu}, 0.1\mathbf{I}_5)$, where \mathbf{I}_5 is the 5×5 identity matrix for $a = 1, 2, 3$. We set each α_y such that the AI is expected to give 60% confidence for the true value $Y_i = y$ and 10% confidence for all other categories. For example, $\alpha_1 = [0.6, 0.1, 0.1, 0.1, 0.1]^\top$. For each sequence i , we randomly sample a row from the covariates matrices, \mathbf{X}_i and \mathbf{U}_i . We assume $\zeta = 1e - 12$ for numerical stability. For settings 1 and 2 we choose thresholds of $T = 0.75, 0.9, \text{ and } 0.99$ (i.e., at least 75%, 90%, and 99% confident respectively).

4.4 Results

We fit each model using 15000 MCMC iterations, the first 10000 of which are discarded as burn-in. The remaining 5000 posterior samples are used for inference and prediction. Convergence was assessed by visual inspection of traceplots and no issues of convergence were detected.

A summary of the RPS results are given in Figure 5. In-sample RPS is best for the full model [50% annotated] (median 0.012) and ordinal-only [50% annotated] (median 0.011). Note that the full model is also making predictions on sequences without any annotated images. The full model [50% annotated] (median 0.136), compositional-only (median 0.136), and ordinal-only [50% annotated] (median 0.136) achieve the best out-of-sample RPS. Thresholding at higher levels does not improve the fit of the model under the maximum setting.

We present MSE for each β coefficient in Table 1. The full model had the lowest MSE for all non-zero β coefficients, while the linear model had slightly lower MSE for β coefficients which equal zero. Coverage for 95% credible intervals (CIs) for β are given in Table 2. Approximately 95% coverage or higher is achieved by the full, ordinal-only, and compositional-only models. The linear and maximum models exhibit under-coverage. Detection, which we define as the proportion of 95% CIs which correctly do not contain

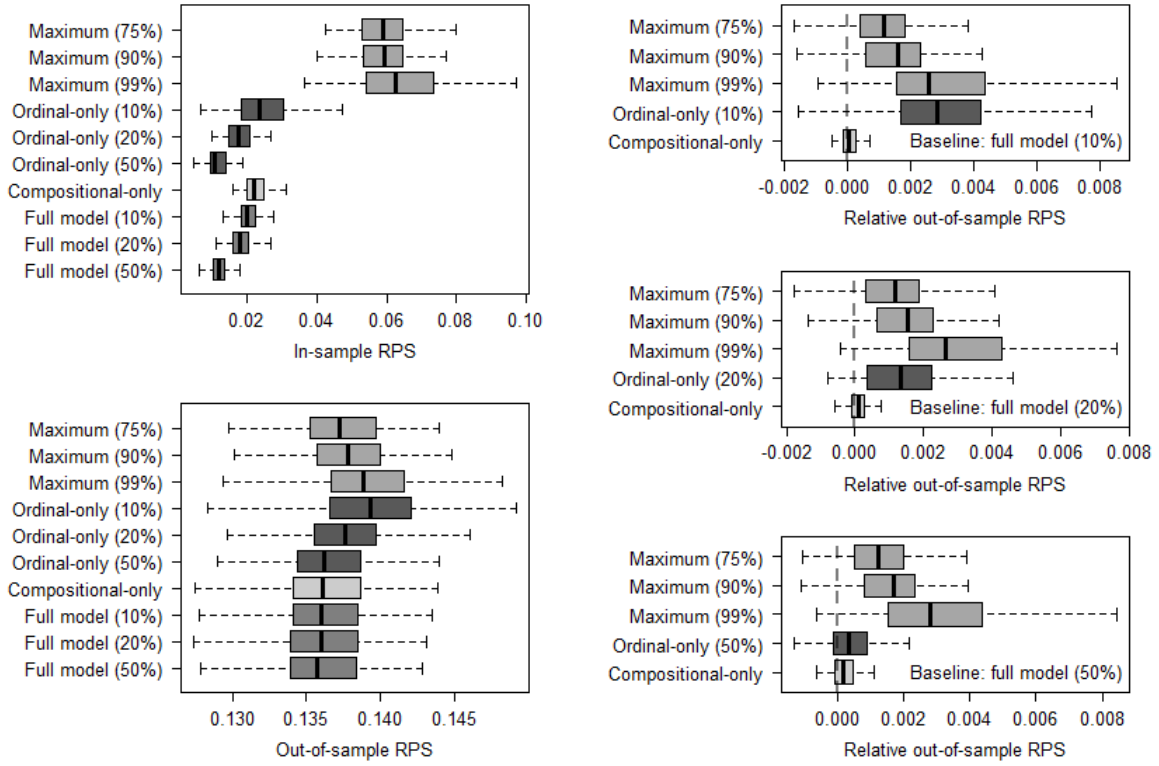


Figure 5: In- and out-of-sample RPS for simulated data (left) and relative out-of-sample ranked probability score (RPS) with respect to the full model (right). The full and ordinal-only models were fit using different percents of annotated images and the maximum model was fit with different thresholds.

	$\beta_1 = 0.2$	$\beta_2 = -0.3$	$\beta_3 = 0.0$	$\beta_4 = 0.0$	$\beta_5 = 0.2$	$\beta_6 = -0.3$
Linear						
Thresholded at 75%	4.53	8.81	2.89	2.79	4.68	6.49
Thresholded at 90%	4.29	8.65	3.82	2.66	4.63	6.10
Thresholded at 99%	4.09	7.90	3.92	3.51	4.84	4.87
Maximum						
Thresholded at 75%	4.67	10.59	3.92	3.81	5.62	7.48
Thresholded at 90%	4.74	11.60	5.32	4.14	6.57	8.58
Thresholded at 99%	6.37	14.61	8.61	7.24	8.25	9.91
Ordinal-only						
10% annotated	8.41	10.81	10.49	11.31	9.05	6.53
20% annotated	5.22	6.16	6.14	5.12	4.63	5.27
50% annotated	3.02	3.98	3.87	4.00	3.58	3.17
Compositional-only	2.68	3.82	3.92	3.95	3.39	2.93
Full model						
10% annotated	2.67	3.64	3.75	3.94	3.15	2.85
20% annotated	2.65	3.41	3.79	3.40	3.21	2.71
50% annotated	2.19	3.11	3.67	3.26	2.95	2.44

Table 1: Mean squared error for each β coefficient for each of the models in settings 1 - 5. True values for each coefficient are given to identify significant and non-significant effects. Mean squared errors are reported by 10^{-3} .

zero for $\beta \neq 0$ and which correctly contain zero for $\beta = 0$, are given in Table 3. The full and compositional-only models achieve approximately 95% detection or higher, while the other models exhibit under-detection, especially the maximum models and ordinal-only with 10%-20% of images annotated. Note that incorrectly detecting significant effects ($\beta \neq 0$) is typically less desirable than incorrectly not detecting significant effects $\beta = 0$.

Across all simulation settings, the full model is competitive with respect to each metric considered, which is not achieved by any of the other models we fit. The compositional-only model performed very similarly to the full model, but was outperformed in in-sample RPS. We find minimal gains from including the manual annotations under these settings in terms of prediction, although they still improved uncertainty quantification. Therefore the full model as proposed in Section 3 has the best performance with respect to estimating the effects of the environmental drivers — including recovering the true values, achieving valid coverage, and detecting differences from zero — and prediction.

	$\beta_1 = 0.2$	$\beta_2 = -0.3$	$\beta_3 = 0.0$	$\beta_4 = 0.0$	$\beta_5 = 0.2$	$\beta_6 = -0.3$
Linear						
Thresholded at 75%	0.79	0.70	0.95	0.94	0.79	0.76
Thresholded at 90%	0.85	0.71	0.94	0.96	0.86	0.85
Thresholded at 99%	0.88	0.84	0.95	0.95	0.84	0.87
Maximum						
Thresholded at 75%	0.87	0.70	0.92	0.93	0.85	0.80
Thresholded at 90%	0.89	0.72	0.95	0.95	0.83	0.81
Thresholded at 99%	0.89	0.81	0.97	0.94	0.91	0.90
Ordinal-only						
10% annotated	1.00	0.94	0.97	0.94	0.96	0.99
20% annotated	0.98	0.94	0.90	0.97	0.98	0.96
50% annotated	0.98	0.93	0.96	0.97	0.92	0.98
Compositional-only	0.99	0.92	0.96	0.95	0.92	0.96
Full model						
10% annotated	0.99	0.94	0.97	0.94	0.95	0.97
20% annotated	0.98	0.96	0.93	0.95	0.94	0.95
50% annotated	0.99	0.95	0.95	0.95	0.95	0.98

Table 2: Empirical coverage based on 95% credible intervals for each β coefficient for model settings 1 - 5.

5 Case study

We fit the proposed model to the Candid Critters camera trap dataset. For comparison, we also fit the linear model thresholded at 90% per expert recommendation. This choice results in 30% of the sequences being discarded. For sequences with more than 30 images, we randomly select a subset of 30 images to limit the computational load. We ran each model for 15000 MCMC iterations, the first 10000 of which are discarded as burn-in and confirmed convergence of the chains by visual inspection of the traceplots of the posterior samples. The 95% CIs for β are given in Figure 6. The coefficient with the largest magnitude corresponds to the indicator variable for whether the deer is a buck in rut. Because bucks tend to gain weight to compete for does during rut, this very strong positive correlation with BCS is expected. We also expect that green, open habitats provide an ideal food source for deer, and so should correspond to a higher BCS [Jones et al., 2010]. Importantly, this effect is detected by the full model but not by the linear

	$\beta_1 = 0.2$	$\beta_2 = -0.3$	$\beta_5 = 0.2$	$\beta_6 = -0.3$	$\beta_3 = 0.0$	$\beta_4 = 0.0$
Linear						
Thresholded at 75%	0.92	0.99	0.90	1.00	0.95	0.94
Thresholded at 90%	0.89	0.99	0.89	1.00	0.94	0.96
Thresholded at 99%	0.86	0.96	0.84	1.00	0.95	0.95
Maximum						
Thresholded at 75%	0.85	0.97	0.80	0.99	0.92	0.93
Thresholded at 90%	0.80	0.89	0.72	0.96	0.95	0.95
Thresholded at 99%	0.66	0.76	0.47	0.89	0.97	0.94
Ordinal-only						
10% annotated	0.61	0.83	0.58	0.93	0.97	0.94
20% annotated	0.83	0.94	0.80	0.98	0.90	0.97
50% annotated	0.96	1.00	0.92	1.00	0.96	0.97
Compositional-only	0.97	1.00	0.95	1.00	0.96	0.95
Full model						
10% annotated	0.97	1.00	0.96	1.00	0.97	0.94
20% annotated	0.97	1.00	0.96	1.00	0.93	0.95
50% annotated	0.99	1.00	0.97	1.00	0.95	0.95

Table 3: Proportion of 95% credible intervals that correctly identify significant (do not cover zero for $\beta \neq 0$) and non-significant (do cover zero for $\beta = 0$) effects for each model setting 1 - 5.

model.

The effects of the remaining covariates on deer health are not well established in ecological literature and therefore provide novel inference. Our model finds that deer relative abundance is positively correlated with BCS, while landscape diversity, green forested habitat, and human population density are negatively correlated. The difference in effects between green and open versus forested habitats likely results from the ability of the deer to access the new vegetation growth.

Predictions are made for a grid of 1264 sites over North Carolina. The NDVI values used to calculate “green and open” and “green and forested” in these predictions are drawn from November 2018. The predicted probability of having a high (4 or 5) body condition for male (i.e. bucks in rut) and female deer are compared in Figure 7. The male deer are predicted to have a much higher BCS overall, and body condition tends to be lower near the mountains and coast.

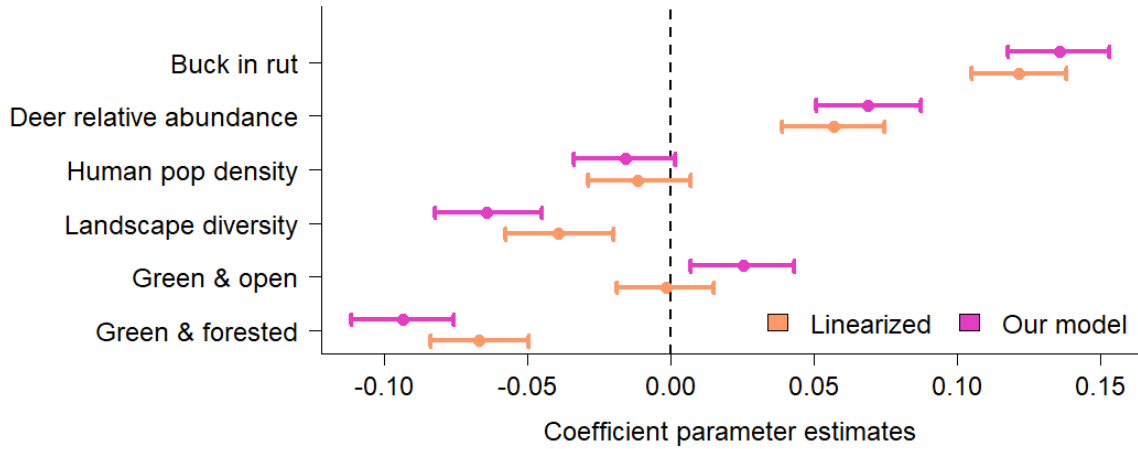


Figure 6: Posterior means and 95% credible intervals for each coefficient β for the Candid Critters analysis under our model compared to the linearized model.

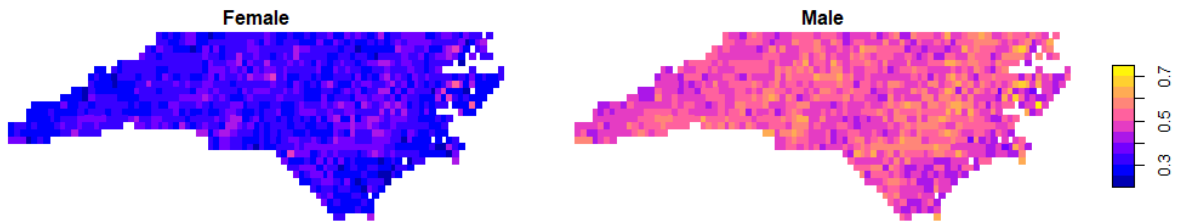


Figure 7: Spatial variation in predictions of probability of having a high (4 or 5) body score for females (left) and males (right) in November 2018.

We also make predictions at several sites of interest which are representative of city, forest, and farm habitats. The covariate values are given in Table 4 and the locations of the selected sites and the predicted probability of an individual deer being in each of the given BCS categories is shown in Figure 8. Male deer are predicted to have higher body condition than female deer during the fall season. Cities and farms have similar results, while forests have a lower proportion of deer with high body condition. This is consistent with the intuition that farmland provides good habitat for deer with a large amount of available vegetation with close proximity to forest habitat.

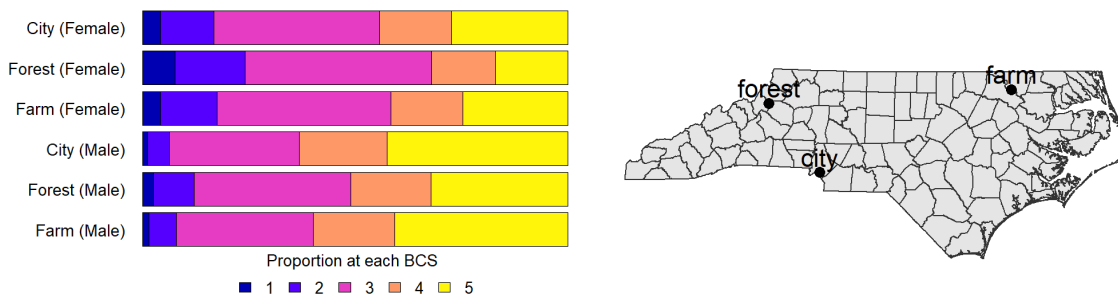


Figure 8: (Left) Posterior predictions of body condition distributions for selected sites for male and female deer during the fall season. (Right) Sites where covariate values were drawn are representative of city, forest, and farm locations.

	Deer relative abundance	Human pop density	Landscape diversity	Green & open	Green
City	0.02	2043.00	0.14	-0.52	-
Forest	0.02	69.70	0.00	-0.88	0
Farm	0.02	72.30	0.03	0.17	-

Table 4: Environmental covariate values for representative sites of a city, forest, and farm location.

6 Discussion

We proposed a novel Bayesian hierarchical framework for the integration of manual annotations and AI confidences from camera trap data. Current approaches often under-utilize or simplify the available data. In particular, they often fail to fully integrate the manual annotations and AI confidences, lack proper uncertainty quantification, and may discard large amounts of data. By jointly modeling manual annotations and AI confidences, we leverage the strengths of both data sources by using the manual annotations to provide calibration and uncertainty quantification, while the AI confidences provide large quantities of inexpensive data spanning broader spatial and environmental extents.

The proposed model is fitted to the Candid Critters camera trap dataset to provide ecological inference with respect to deer BCS and environmental drivers across North Carolina. A simplified linear model was also fitted for comparison. Both models suggest a strong positive correlation between bucks in rut and BCS, as is expected from basic deer biology. The proposed model also finds that BCS is positively correlated with green open

habitat, while the linear model does not detect a significant relationship. Our model also provides novel inference, suggesting that BCS is positively correlated with deer relative abundance and negatively correlated with landscape diversity, green forested habitat, and possibly human population density. Future work looks to expand our analysis to Snapshot USA data, a larger camera trap study which spans the United States [Rooney et al., 2025]. This would allow us to make inference on the effect of other important health indices, such as Chronic Wasting Disease, a prion disease which has been spreading across the country and internationally [U.S. Centers for Disease Control and Prevention, 2024].

Utilizing AI-integrated camera trap data opens up new areas of exploration in ecology. Body condition in deer is a mostly unexplored area of research. The existing studies are limited by the cost of data collection. For example, Simard et al. [2014] conduct a similar analysis of the relationship between environmental drivers and deer body condition in the fall. They consider deer collected by hunters, leading to a much smaller and possibly biased sample. Our results are similar in finding that body condition is lower in female deer, although they find that body condition is lower in areas with high deer density, whereas we found a positive correlation.

The benefit of the manual annotations is that they enable calibration of the joint model, a critical step in ensuring valid inference. However, one limitation we found in our analysis using the proposed model is that a high proportion of manual annotations are necessary. In fact, the compositional-only model was shown to be highly competitive with respect to the other simplified settings. This result may not be robust to other camera trap analyses and should be explored in future studies with different response types, such as disease conditions. We predict that the effect of the manual annotations depends in part on how well the AI model is calibrated.

Another limitation of using AI predictions is the inability to account for sequences containing multiple deer. This is due to the difficulty associated with identifying and tracking individual deer between images. A potential solution would be to randomly

select one image from each sequence with multiple deer. Models that can incorporate multiple animals are particularly important for species that commonly travel in groups, such as white-tailed deer, elk, and wild boar.

More extensive methodological development entails extending the approach to occupancy or abundance modeling which will focus on species identification. The branching taxonomic structure defining similarity between species requires statistical novelty beyond the ordinal latent variable modeling for BCS. In particular, we expect that AI models trained to identify species will have a harder time distinguishing closely related species than distantly related species. It is also of interest to perform inference on multiple taxonomic levels, such as species or genus level, although current models are limited to one level. Manual annotations may be more valuable for this type of model, and sequential design could be used to guide such annotation schemes. Sequential design or active learning approaches inform model design by optimizing the labeling of data (e.g., the species identity) with respect to both model inference and uniformly sampling the available data. This is an area of active research and has not yet been applied to occupancy and abundance models.

Data availability

The code for fitting the model and simulating data will be made available on GitHub upon acceptance of the manuscript.

7 T

he first author was supported in part by the NSF-RTG: Uncertainty Quantification in Life Sciences (UQ4Life) (DMS-2342344) and Summer One Health Internship on Wildlife Health offered by the North Carolina Museum of Natural Sciences in collaboration with

the North Carolina State Global One Health Academy. The manual annotations, including for use in training the AI model, were in part provided by the Seed Funding Grant, NCSU Office of University Interdisciplinary Programs.

References

- Benjamin R. Goldstein, Alex J. Jensen, Roland Kays, Michael V. Cove, William J. McShea, Brigit Rooney, Elizabeth M. Kierepka, and Krishna Pacifici. Guidelines for estimating occupancy from autocorrelated camera trap detections. *Methods in Ecology and Evolution*, 15(7):1177–1191, 2024. doi: <https://doi.org/10.1111/2041-210X.14359>. URL <https://besjournals.onlinelibrary.wiley.com/doi/abs/10.1111/2041-210X.14359>.
- Erin M Schliep, Alan E Gelfand, Christopher W Clark, Charles A Mayo, Brigid McKenna, Susan E Parks, Tina M Yack, and Robert S Schick. Assessing marine mammal abundance: A novel data fusion. *The Annals of Applied Statistics*, 18(4):3071–3090, 2024.
- Arthur B. Muneza, Waldemar Ortiz-Calo, Craig Packer, Jeremy J. Cusack, Trevor Jones, Meredith S. Palmer, Alexandra Swanson, Margaret Kosmala, Amy J. Dickman, David W. Macdonald, and Robert A. Montgomery. Quantifying the severity of giraffe skin disease via photogrammetry analysis of camera trap data. *Journal of Wildlife Diseases*, 55(4):770–781, 10 2019. ISSN 0090-3558. doi: 10.7589/2018-06-149. URL <https://doi.org/10.7589/2018-06-149>.
- Elise M. Ringwaldt, Jessie C. Buettel, Scott Carver, and Barry W. Brook. Epidemiological dynamics of a visually apparent disease: Camera trapping and machine-learning applied to rumpwear in the common brushtail possum. *Integrative Zoology*, 2025. doi: <https://doi.org/10.1111/1749-4877.12995>.
- Scott Leorna and Todd Brinkman. Human vs. machine: Detecting wildlife

- in camera trap images. *Ecological Informatics*, 72:101876, 2022. ISSN 1574-9541. doi: <https://doi.org/10.1016/j.ecoinf.2022.101876>. URL <https://www.sciencedirect.com/science/article/pii/S1574954122003260>.
- Zackary J Delisle, Elizabeth A Flaherty, Mackenzie R Nobbe, Cole M Wzientek, and Robert K Swihart. Next-generation camera trapping: systematic review of historic trends suggests keys to expanded research applications in ecology and conservation. *Frontiers in Ecology and Evolution*, 9:617996, 2021.
- J. Christopher D. Terry, Helen E. Roy, and Tom A. August. Thinking like a naturalist: Enhancing computer vision of citizen science images by harnessing contextual data. *Methods in Ecology and Evolution*, 11(2):303–315, 2020. doi: <https://doi.org/10.1111/2041-210X.13335>. URL <https://besjournals.onlinelibrary.wiley.com/doi/abs/10.1111/2041-210X.13335>.
- Mateus Braga Oliveira, Heder Soares Bernardino, Alex Borges Vieira, and Douglas A. Augusto. Classification of animal species via deep neural networks and species distribution modeling: a systematic review. *Artificial Intelligence Review*, 58(230), 2025. doi: <https://doi.org/10.1007/s10462-024-11074-w>.
- Margarita Mulero-Pázmány, Cristóbal Barba-González Sandro Hurtado, María Luisa Antequera-Gómez, Francisco Díaz-Ruiz, Raimundo Real, Ismael Navas-Delgado, and José’ F. Aldana-Montes. Addressing significant challenges for animal detection in camera trap images: a novel deep learning-based approach. *Scientific Reports*, 15(16191), 2025. doi: <https://doi.org/10.1038/s41598-025-90249-z>.
- Maik Henrich, Mercedes Burgueño, Jacqueline Hoyer, Timm Haucke, Volker Steinhage, Hjalmar S. Kühl, and Marco Heurich. A semi-automated camera trap distance sampling approach for population density estimation. *Remote Sensing in Ecology*

- and Conservation*, 10(2):156–171, 2024. doi: <https://doi.org/10.1002/rse2.362>. URL <https://zslpublications.onlinelibrary.wiley.com/doi/abs/10.1002/rse2.362>.
- Robert C. Lonsinger, Marlin M. Dart, Randy T. Larsen, and Robert N. Knight. Efficacy of machine learning image classification for automated occupancy-based monitoring. *Remote Sensing in Ecology and Conservation*, 10(1):56–71, 2024. doi: <https://doi.org/10.1002/rse2.356>. URL <https://zslpublications.onlinelibrary.wiley.com/doi/abs/10.1002/rse2.356>.
- Amber Cowans, Xavier Lambin, Darragh Hare, and Chris Sutherland. Improving the integration of artificial intelligence into existing ecological inference workflows. *Methods in Ecology and Evolution*, 2024. doi: <https://doi.org/10.1111/2041-210X.14485>. URL <https://besjournals.onlinelibrary.wiley.com/doi/abs/10.1111/2041-210X.14485>.
- Tessa A. Rhinehart, Daniel Turek, and Justin Kitzes. A continuous-score occupancy model that incorporates uncertain machine learning output from autonomous biodiversity surveys. *Methods in Ecology and Evolution*, 13(8):1778–1789, 2022. doi: <https://doi.org/10.1111/2041-210X.13905>. URL <https://besjournals.onlinelibrary.wiley.com/doi/abs/10.1111/2041-210X.13905>.
- Jerry S Cole, Nicole L Michel, Shane A Emerson, and Rodney B Siegel. Automated bird sound classifications of long-duration recordings produce occupancy model outputs similar to manually annotated data. *Ornithological Applications*, 124(2):duac003, 04 2022. ISSN 0010-5422. doi: 10.1093/ornithapp/duac003. URL <https://doi.org/10.1093/ornithapp/duac003>.
- Congtian Lin, Xiongwei Huang, Jiangning Wang, Tianyu Xi, and Liqiang Ji. Learning niche features to improve image-based species identification. *Ecological Informatics*, 61:101217, 2021. ISSN 1574-

9541. doi: <https://doi.org/10.1016/j.ecoinf.2021.101217>. URL <https://www.sciencedirect.com/science/article/pii/S157495412100008X>.
- Michael R. Schwob, Mevin B. Hooten, Nicholas M. Calzada, and Timothy H. Keitt. Spatial hyperspheric models for compositional data, 2025. URL <https://arxiv.org/abs/2410.03648>.
- Xiaoping Feng, Jun Zhu, Pei-Sheng Lin, and Michelle M. Steen-Adams. Composite likelihood approach to the regression analysis of spatial multivariate ordinal data and spatial compositional data with exact zero values. *Environmental and Ecological Statistics*, 24:39–68, 2017. doi: <https://doi.org/10.1007/s10651-016-0360-0>.
- Justin Kitzes, Lauren Chronister, Chapin Czarnecki, Cameron Fiss, Louis Freeland-Haynes, Brooke D. Goodman, Sam Lapp, R. Patrick Lyon, Hannah Nossan, Tessa A. Rhinehart, Santiago Ruiz Guzman, Alexandra Syunkova, and Leonardo Viotti. Integrating ai models into ecological research workflows: The case of terrestrial bioacoustics. *Methods in Ecology and Evolution*, 2025. doi: <https://doi.org/10.1111/2041-210X.70133>. URL <https://besjournals.onlinelibrary.wiley.com/doi/abs/10.1111/2041-210X.70133>.
- Gaspard Dussert, Simon Chamaille-Jammes, Stéphane Dray, and Vincent Miele. Being confident in confidence scores: calibration in deep learning models for camera trap image sequences. *Remote Sensing in Ecology and Conservation*, 11(1):88–99, 2025. doi: <https://doi.org/10.1002/rse2.412>. URL <https://zslpublications.onlinelibrary.wiley.com/doi/abs/10.1002/rse2.412>.
- Lena Ware, C. Lisa Mahon, Logan McLeod, and Jean-François Jetté. Artificial intelligence (birdnet) supplements manual methods to maximize bird species richness from acoustic data sets generated from regional monitoring. *Canadian Jour-*

nal of Zoology, 101(12):1031–1051, 2023. doi: 10.1139/cjz-2023-0044. URL <https://doi.org/10.1139/cjz-2023-0044>.

Connor M. Wood, Jacob Socolar, Stefan Kahl, M. Zachariah Peery, Philip Chaon, Kevin Kelly, Robert A. Koch, Sarah C. Sawyer, and Holger Klinck. A scalable and transferable approach to combining emerging conservation technologies to identify biodiversity change after large disturbances. *Journal of Applied Ecology*, 61(4):797–808, 2024. doi: <https://doi.org/10.1111/1365-2664.14579>. URL <https://besjournals.onlinelibrary.wiley.com/doi/abs/10.1111/1365-2664.14579>.

Jeffrey W. Doser, Andrew O. Finley, Aaron S. Weed, and Elise F. Zipkin. Integrating automated acoustic vocalization data and point count surveys for estimation of bird abundance. *Methods in Ecology and Evolution*, 12(6):1040–1049, 2021. doi: <https://doi.org/10.1111/2041-210X.13578>. URL <https://besjournals.onlinelibrary.wiley.com/doi/abs/10.1111/2041-210X.13578>.

Andrii Zaiats, T. Trevor Caughlin, Jennyffer Cruz, David S. Pilliod, Megan E. Cattau, Rongsong Liu, Richard Rachman, Maisha Maliha, Donna Delparte, and John D. J. Clare. Propagating observation errors to enable scalable and rigorous enumeration of plant population abundance with aerial imagery. *Methods in Ecology and Evolution*, 15(11):2074–2086, 2024. doi: <https://doi.org/10.1111/2041-210X.14421>. URL <https://besjournals.onlinelibrary.wiley.com/doi/abs/10.1111/2041-210X.14421>.

Monica Lasky, Arielle Parsons, Stephanie Schuttler, Alexandra Mash, Lincoln Larson, Ben Norton, Brent Pease, Hailey Boone, Lisa Gatens, and Roland Kays. Candid critters: Challenges and solutions in a large-scale citizen science camera trap project. *Citizen Science: Theory and Practice*, Feb 2021.

Rachel A. Smiley. Beyond capture: Development and validation of a method to assess

body condition in mule deer (*Odocoileus hemionus*) using camera traps. Honors scholar thesis, University of Connecticut, 2017.

Amanda M. McGraw, Daniel J. Storm, Dustin R. Bronson, and Teresa Pearson. Habitat and weather influence body condition in white-tailed deer, Wisconsin, USA. *The Journal of Wildlife Management*, 86(2):e22176, 2022. doi: <https://doi.org/10.1002/jwmg.22176>. URL <https://wildlife.onlinelibrary.wiley.com/doi/abs/10.1002/jwmg.22176>.

Mohammad Alyetama and Matthew Snider. Dhs. <https://github.com/Alyetama/dhs>, 2024. Accessed: 2024-07-18.

Roland Kays, Matthew H. Snider, George Hess, Michael V. Cove, Alex Jensen, Hila Shammon, William J. McShea, Brigit Rooney, Maximilian L. Allen, Charles E. Pekins, Christopher C. Wilmers, Mary E. Pendergast, Austin M. Green, Justin Suraci, Matthew S. Leslie, Sophie Nasrallah, Dan Farkas, Mark Jordan, Melissa Grigione, Michael C. LaScaleia, Miranda L. Davis, Chris Hansen, Josh Millsbaugh, Jesse S. Lewis, Michael Havrda, Robert Long, Kathryn R. Remine, Kodi J. Jaspers, Diana J. R. Lafferty, Tru Hubbard, Colin E. Studds, Erika L. Barthelmess, Katherine Andy, Andrea Romero, Brian J. O'Neill, Melissa T. R. Hawkins, Jason V. Lombardi, Maksim Sergeev, M. Caitlin Fisher-Reid, Michael S. Rentz, Christopher Nagy, Jon M. Davenport, Christine C. Rega-Brodsky, Cara L. Appel, Damon B. Lesmeister, Sean T. Giery, Christopher A. Whittier, Jesse M. Alston, Chris Sutherland, Christopher Rota, Thomas Murphy, Thomas E. Lee Jr., Alessio Mortelliti, Dylan L. Bergman, Justin A. Compton, Brian D. Gerber, Jess Burr, Kylie Rezendes, Brett A. DeGregorio, Nathaniel H. Wehr, John F. Benson, M. Teague O'Mara, David S. Jachowski, Morgan Gray, Dean E. Beyer Jr., Jerrold L. Belant, Robert V. Horan III, Robert C. Lonsinger, Kellie M. Kuhn, Steven C. M. Hasstedt, Marketa Zimova, Sophie M. Moore, Daniel J. Herrera, Sarah Fritts, Andrew J. Edelman, Elizabeth A. Flaherty, Tyler R.

Petroelje, Sean A. Neiswenter, Derek R. Risch, Fabiola Iannarilli, Marius van der Merwe, Sean P. Maher, Zach J. Farris, Stephen L. Webb, David S. Mason, Marcus A. Lashley, Andrew M. Wilson, John P. Vanek, Samuel R. Wehr, L. Mike Conner, James C. Beasley, Helen L. Bontrager, Carolina Baruzzi, Susan N. Ellis-Felege, Mike D. Proctor, Jan Schipper, Katherine C. B. Weiss, Andrea K. Darracq, Evan G. Barr, Peter D. Alexander, Çağan H. Şekercioğlu, Daniel A. Bogan, Christopher M. Schalk, Jean E. Fantle-Lepczyk, Christopher A. Lepczyk, Scott LaPoint, Laura S. Whipple, Helen Ivy Rowe, Kayleigh Mullen, Tori Bird, Adam Zorn, LaRoy Brandt, Richard G. Lathrop, Craig McCain, Anthony P. Crupi, James Clark, and Arielle Parsons. Climate, food and humans predict communities of mammals in the united states. *Diversity and Distributions*, 30(9):e13900, 2024. doi: <https://doi.org/10.1111/ddi.13900>. URL <https://onlinelibrary.wiley.com/doi/abs/10.1111/ddi.13900>.

U.S. Census Bureau. Annual estimates of the resident population for counties: April 1, 2020 to July 1, 2024 (co-est2024-pop). <https://www.census.gov/data/tables/time-series/demo/popest/2020s-counties-total.html>. Accessed: 2024-03-04.

Martin Jung, Prabhat Raj Dahal, Stuart HM Butchart, Paul F Donald, Xavier De Lamo, Myroslava Lesiv, Valerie Kapos, Carlo Rondinini, and Piero Visconti. A global map of terrestrial habitat types. *Scientific data*, 7(1):256, 2020. doi: <https://doi.org/10.1038/s41597-020-00599-8>.

S Dodge, G Bohrer, R Weinzierl, S C Davidson, R Kays, D Douglas, S Cruz, J Han, D Brandes, and M Wilkelski. The environmental-data automated track annotation (env-data) system: linking animal tracks with environmental data. <https://doi.org/10.1186/2051-3933-1-3>, 2013.

Joseph O. Sexton, Xiao-Peng Song, Min Feng, Praveen Noojipady, Anupam Anand,

- Chengquan Huang, Do-Hyung Kim, Kathrine M. Collins, Saurabh Channan, Charlene DiMiceli, and John R. Townshend. Global, 30-m resolution continuous fields of tree cover: Landsat-based rescaling of modis vegetation continuous fields with lidar-based estimates of error. *International Journal of Digital Earth*, 6(5):427–448, 2013. doi: 10.1080/17538947.2013.786146. URL <https://doi.org/10.1080/17538947.2013.786146>.
- James H Albert and Siddhartha Chib. Bayesian analysis of binary and polychotomous response data. *Journal of the American statistical Association*, 88(422):669–679, 1993.
- Tilmann Gneiting and Adrian E. Raftery. Strictly proper scoring rules, prediction, and estimation. *Journal of the American Statistical Association*, 102(477):359–378, 2007. doi: 10.1198/016214506000001437. URL <https://doi.org/10.1198/016214506000001437>.
- Phillip D. Jones, Bronson K. Strickland, Stephen Demarais, Brian J. Rude, Scott L. Edwards, and James P. Muir. Soils and forage quality as predictors of white-tailed deer *odocoileus virginianus* morphometrics. *Wildlife Biology*, 16(4):430–439, 2010. doi: <https://doi.org/10.2981/10-041>. URL <https://nsojournals.onlinelibrary.wiley.com/doi/abs/10.2981/10-041>.
- Brigit Rooney, Roland Kays, Michael V. Cove, Alex Jensen, Benjamin R. Goldstein, Christopher Pate, Paula Castiblanco, Maggie E. Abell, Jessie Adley, Briana Agenbroad, Adam A. Ahlers, Peter D. Alexander, David Allen, Maximilian L. Allen, Jesse M. Alston, Mohammad Alyetama, Thomas L. Anderson, Raul Andrade, Christine Anhalt-Depies, Cara L. Appel, Leslie Armendariz, Christopher R. Ayers, Amy B. Baird, Cara Bak, Griffin Bandler, Erin E. Barding, Evan G. Barr, Carolina Baruzzi, Kelli Bashaw, Silas C. Beers, Jerrold L. Belant, Emma Bell, John F. Benson, Anna Berg, Dylan L. Bergman, Brandon M. Bernhardt, Meagan A. Bethel, Tori Bird,

Amanda B. Bishop, Daniel A. Bogan, LaRoy Brandt, Levin C. Brandt, Aidan B. Branney, Chloe Bratton, Claire E. Bresnan, Jarred M. Brooke, Erin K. Buchholtz, Frances Buderman, Alexandra D. Burnett, Emily E. Burns, Dominique A. Byrd, Susan A. Cannella, Kathleen A. Carey, William A. Carlile, Kellie L. Carter, Brenna J. Cassidy, Ivan Castro-Arellano, Sara Cendejas-Zarelli, Nilanjan Chatterjee, Amanda E. Cheeseman, Cary Chevalier, M. Colter Chitwood, Petros Chrysafis, Bret Aaron Collier, D. Parks Collins, Justin A. Compton, Rhea Cone, L. Mike Conner, Brianna L. Cook, Olivia G. Cosby, Stephanie S. Coster, Anthony P. Crupi, Andrea K. Darracq, Jon M. Davenport, Devin Davis, Drew R. Davis, Miranda L. Davis, Rebecca J. Davis, Brett A. DeGregorio, Anant Deshwal, Kyle D. Dougherty, Art Drauglis, Caleb J. Durbin, Andrew J. Edelman, Valerie Elder, Blakely Eller, E. Hance Ellington, Susan N. Ellis-Felege, Caroline N. Ellison, Jean E. Fantle-Lepczyk, Jonathan J. Farr, Zach J. Farris, Shannon P. Finnegan, M. Caitlin Fisher-Reid, Elizabeth A. Flaherty, Gabriela Franzoi Dri, Sarah Fritts, Jeremy Fuller, Travis Gallo, Laken S. Ganoe, Carissa N. Ganong, Ricky Garibay, Brian D. Gerber, Francis D. Gerraty, Sean T. Giery, Selena M. Gilyot, Jessica L. Glasscock, Ben Goldfarb, Louis E. Good, Gracie Granados, Austin M. Green, Jasmine K. Grewal, Andrew Grusenmeyer, Joseph M. Guthrie, Matthew T. Hallett, Chris Hansen, Lonnie P. Hansen, Clae Hanson, Eamon J. Harrity, Steven C. M. Hasstedt, Mark Hebblewhite, Daniel J. Herrera, Angela Holland, Brigit R. Humphreys, Heide D. Island, Alexander R. Jack, Emily P. Johansson, Alex M. Johnson, Luanne Johnson, Tamara L. Johnstone-Yellin, Maria Luisa S. P. Jorge, Willaine Kahano, Michael A. Kinsey, Brier E. Klossing, Travis W. Knowles, Molly M. Koeck, John L. Koprowski, Kellie M. Kuhn, Erin K. Kuprewicz, Diana J. R. Lafferty, Jessica A. Lamberton-Moreno, Travis J. Land, Avy M. Langston, Scott LaPoint, Erin N. Largent, Marcus A. Lashley, Richard G. Lathrop, Thomas E. Lee Jr, Christopher A. Lepczyk, Damon B. Lesmeister, Carissa Leung, Jason V. Lombardi, Robert Long, Robert C. Lonsinger, Isaac Lord, Steven S. Madere, Sean P. Maher, Jenifer A. Mallinoff, Andres Martinez,

David S. Mason, Heather A. Mathewson, Amy E. Mayer, Kyle P. McCarthy, Shawn F. McCracken, Brandon McDonald, Brendan McGarry, Sierra T. McMurry, Leah E. McTigue, Brianna Marie Mena, Margaret Mercer, Margaret R. Merz, Sophie Millar, Geoffrey D. Miller, Joshua J. Millspaugh, Remington J. Moll, Tony W. Mong, Javier D. Monzón, John C. Moore, Alessio Mortelliti, Kelton W. Mote, Kayleigh Mullen, Alexis Mychajliw, Christopher Nagy, Sean A. Neiswenter, Drew R. Neyland, Laura P. Nicholson, M. Teague O'Mara, Brian J. O'Neill, Elizabeth A. Olson, Michael J. Orgill, Gabriela Palomo-Munoz, Shawn M. Parsons, Lorelei E. Patrick, Jessica R. Patterson, David L. Pearce, Mary E. Pendergast, Bianca S. Perla, Tyler R. Petroelje, Henry Pliske, Mairi K. P. Poisson, Melissa R. Price, Mike D. Proctor, Nathan J. Proudman, Janet L. Rachlow, Ramon E. Ramos, Miguel Reabold, Joseph Redinger, Adar E. Reed, Christine C. Rega-Brodsky, Evan Rehm, Kathryn R. Remine, Michael S. Rentz, Elizabeth Ridder, Derek R. Risch, Lydia L. Robbins, Justin P. Roemer, Andrea Romero, Christopher Rota, Christopher M. Schalk, Bradley D. Scholten, Christina L. Scott, Brandon M. Scurlock, Maksim Sergeyev, William J. Severud, Jennifer Sevin, Hila Shamon, Conan Sharp, Michael Shaw, Veronica Siverls-Dunham, Austin B. Smith, Daniel S. Smith, Matthew H. Snider, Daniel A. Sossover, Adia R. Sovie, J. Alan Sparks, Jessica Speiser, Matthew T. Springer, Jared L. Spurlin, Eric A. Steinkamp, Jennifer L. Stenglein, Joanne Stewart Kloker, Cassie M. Stitzman, Michael Stokes, Khloey Stringer, Johnathon Stutzman, Daniel S. Sullins, Cassandra Sullivan, Noah B. Sullivan, Evan P. Tanner, Ashley M. Tanner, Emily B. Thornock, Jack Titus, Jacquelyn M. Tleimat, Kenny Toomey, Luke T. Toussaint, Michael Uribe, Marius Van der Merwe, Dakota J. Van Parys, John P. Vanek, Johanna Varner, Brienna V. Walker, Cody Wallace, David Ward, Bethany H. Warner, Derick T. Warren, Joanne R. Wasdin, Stephen L. Webb, Katelyn L. Wehr, Nathaniel H. Wehr, Emily G. Weigel, Ty J. Werdel, Laura S. Whipple, Christopher A. Whittier, Chloe Wiersema, Andrew Mark Wilson, Margaret F. H. Wilson, Alexander J. Wolf, Justin P. Wolford, David W. Wolfson, Daniel J. Woolsey,

Matthew Alan Wuensch, Gloria Xu, Kerry L. Yurewicz, Veronica Zanco, Marketa Zimova, Adam Zorn, and William J. McShea. Snapshot usa 2019–2023: The first five years of data from a coordinated camera trap survey of the united states. *Global Ecology and Biogeography*, 34(1):e13941, 2025. doi: <https://doi.org/10.1111/geb.13941>. URL <https://onlinelibrary.wiley.com/doi/abs/10.1111/geb.13941>. e13941 GEB-2024-0441.R1.

U.S. Centers for Disease Control and Prevention. Chronic wasting disease in animals. <https://www.cdc.gov/chronic-wasting/animals/index.html>, 2024. Accessed: 2024-12-01.

Anouk Simard, Jean Huot, Sonia De Bellefeuille, and Steeve D. Côté. Influences of habitat composition, plant phenology, and population density on autumn indices of body condition in a northern white-tailed deer population. *Wildlife Monographs*, 187(1):1–28, 2014. doi: <https://doi.org/10.1002/wmon.1010>. URL <https://wildlife.onlinelibrary.wiley.com/doi/abs/10.1002/wmon.1010>.

Supplement

S.1 Notation

Model notation is organized in Table 5.

S.2 Sampling approach

A Gibbs step is used to sample Y_i given \mathbf{Z}_i and \mathbf{C}_i . Using Bayes rule, as well as the independence of Z_i and C_i given Y_i and between sequences given the parameters, for any sequence $i = 1, \dots, N$,

$$\begin{aligned} \mathbb{P}(Y_i = y | \mathbf{Z}_i, \mathbf{C}_i, \beta_0, \boldsymbol{\beta}, \boldsymbol{\theta}, \boldsymbol{\nu}, \boldsymbol{\phi}, \boldsymbol{\alpha}, \omega_0, \boldsymbol{\omega}) \\ = \frac{f_Y(Y_i = y | \beta_0, \boldsymbol{\beta}, \boldsymbol{\theta}) f_Z(\mathbf{Z}_i | Y_i = y, \boldsymbol{\nu}, \boldsymbol{\phi}) f_C(\mathbf{C}_i | Y_i = y, \boldsymbol{\alpha}, \omega_0, \boldsymbol{\omega})}{\sum_{\ell=1}^L f_Y(Y_i = \ell | \beta_0, \boldsymbol{\beta}, \boldsymbol{\theta}) f_Z(\mathbf{Z}_i | Y_i = \ell, \boldsymbol{\nu}, \boldsymbol{\phi}) f_C(\mathbf{C}_i | Y_i = \ell, \boldsymbol{\alpha}, \omega_0, \boldsymbol{\omega})} \end{aligned} \quad (4)$$

where

$$f_Z(\mathbf{Z}_i | Y_i, \boldsymbol{\nu}, \boldsymbol{\phi}) = \prod_{k \in \Lambda_i^Y} f_Z(Z_{i,k} | Y_i, \boldsymbol{\nu}, \boldsymbol{\phi})$$

and

$$f_C(\mathbf{C}_i | Y_i, \boldsymbol{\alpha}, \omega_0, \boldsymbol{\omega}) = \prod_{k \in \Lambda_i^C} f_C(C_{i,k} | Y_i, \boldsymbol{\alpha}, \omega_0, \boldsymbol{\omega}).$$

Note that $Y_i | \mathbf{Z}_i, \mathbf{C}_i, \dots$ are still independently distributed.

Each parameter vector $\boldsymbol{\beta}$, $\tilde{\boldsymbol{\theta}}$, and $\boldsymbol{\omega}$ is sampled in block. Parameter vectors $\tilde{\boldsymbol{\phi}}_y$ and $\boldsymbol{\alpha}_y$ are sampled together for each category y , while each element of $\boldsymbol{\nu}$ and $\tilde{\boldsymbol{\nu}}$ are sampled univariately.

S.3 Ranked probability score

To compare model fits, we use the ranked probability score (RPS) as described by Gneiting and Raftery [2007]. It is a proper scoring rule, meaning that it rewards both calibra-

tion and sharpness. For our purposes this means that it rewards statistical consistency between the posterior and true values as well as tight credible intervals. We apply RPS using the equation

$$\text{RPS}(\hat{p}, p) = \frac{1}{L-1} \sum_{\ell=1}^{L-1} \left(\sum_{k=1}^{\ell} \hat{p}(k) - p(k) \right)^2 \quad (5)$$

where p and \hat{p} are densities for a discrete random variable. Note that this corresponds to the ℓ_2 distance between the two distributions. To summarize the RPS for each model we take the mean over all sequences.

Parameter	Dimensions	Meaning
N, R	positive integers	number of sequences and images
r_i	integer	number of images in sequence i
Λ_i^Z, Λ_i^C	up to r_i -length vectors	indices of the images in sequence i with manual annotations and AI confidences, respectively
L	positive integer	number of categories
p, q	positive integers	number of environmental and image-quality covariates
A	positive integer	number of annotators
Y_i	one of $\{1, \dots, L\}$	true latent BCS for sequence i
$Z_{i,k}$	one of $\{1, \dots, L\}$	ordinal BCS annotation for image k of sequence i
$\mathbf{C}_{i,k}$	L -length vector	compositional AI confidences for image k of sequence i
\mathbf{X}_i	p -length vector	environmental covariates for sequence i
$\mathbf{U}_{i,k}$	q -length vector	image-quality covariates for image k of sequence i
$a_{i,k}$	integer	identity of the annotator for image k of sequence i
β_0	real number	intercept coefficient for true latent BCS
$\boldsymbol{\beta}$	p -length vector	coefficients mapping environmental covariates to true latent BCS
$\boldsymbol{\theta}$	$(L + 1)$ -length vector	cutoffs for Y ; $-\infty = \theta_0 < 0 = \theta_1 < \dots < \theta_{L-1} < \theta_L = \infty$
$\tilde{\boldsymbol{\theta}}$	$(L - 2)$ -length vector	reparameterization of $\boldsymbol{\theta}$; $\theta_y = \theta_{y-1} + e^{\tilde{\theta}_y}$ for $y \in \{2, \dots, L - 1\}$
$\boldsymbol{\phi}_y$	$(L + 1)$ -length vector	cutoffs for Z_i when $Y_i = y$; $-\infty = \phi_{y,0} < 0 = \phi_{y,1} < \dots < \phi_{y,L-1} < \phi_{y,L} = \infty$
$\tilde{\boldsymbol{\phi}}_y$	$(L - 2)$ -length vector	reparameterization of $\boldsymbol{\phi}_y$; $\phi_{y,z} = \phi_{y,z-1} + e^{\tilde{\phi}_{y,z}}$ for $z \in \{2, \dots, L - 1\}$
$\nu_y^{(a)}$	real number	mean of latent annotation normal random variable for annotator a when $Y_i = y$
$\tilde{\nu}_y$	real number	latent mean parameter for $\nu_y^{(1)}, \dots, \nu_y^{(A)}$
$\boldsymbol{\alpha}_y$	L -length vector	means for compositional responses if $Y_i = y$; $\boldsymbol{\alpha}_y$ in $(L - 1)$ -simplex
ω_0	real number	(logged) intercept for precision of compositional responses
$\boldsymbol{\omega}$	q -length vector	image-quality coefficients for precision of compositional responses

Table 5: Table of model notation.